Techniques for Modeling Fiber Laser Amplifiers

Jay Gopalakrishnan, Tathagata Goswami, and Jacob Grosek

Abstract Numerical techniques for simulation of electromagnetic wave propagation within fiber amplifiers are discussed. Since a full-featured simulation using the Maxwell system on a realistic fiber is beyond reach, simplified models using Coupled Mode Theory (CMT) form the state of the art. This work presents a novel concept of an *equivalent short fiber,* namely an artificial fiber which imitates a longer fiber in essential characteristics. A CMT simulation on an equivalent short fiber requires only a fraction of the computational resources needed to simulate the full length fiber.

1 Fiber Amplifiers

The ability of solid-state fiber laser amplifiers to deliver high output power has been exploited and studied over the last few decades [4]. Currently, the main roadblock to power scaling these amplifiers is the transverse mode instability (TMI), a sudden breakdown in beam quality at high power operation, first observed experimentally [2]. These observations have led to intensive speculations on the cause of TMI, the prevailing theory being that the cause is a temperature-induced grating. Reliable numerical simulation of TMI and other nonlinear optical effects within fibers can provide important insights for validating or rejecting various physical hypotheses put forth to explain these effects. The simulation techniques must however be able to numerically solve the field propagation within a long fiber a vast number of times.

J. Gopalakrishnan (✉) · T. Goswami
Portland State University, Portland, OR, USA
e-mail: gjay@pdx.edu; tgoswami@pdx.edu

J. Grosek
Directed Energy Directorate, Air Force Research Laboratory, Kirtland Air Force Base, Albuquerque, NM, USA
e-mail: jacob.grosek.1@us.af.mil

G. Nicosia, V. Romano (eds.), *Scientific Computing in Electrical Engineering*, Mathematics in Industry 32, https://doi.org/10.1007/978-3-030-44101-2_5

While numerical modeling of fiber amplifiers has been effectively used by many [5, 6, 9], accurate simulation of full length fibers remains cumbersome due to its high demands on computational resources and long simulation times. A full Maxwell simulation of Raman gain in a fiber was attempted in [7]: more than five million degrees of freedom was needed to simulate a fiber 80 wavelengths long (less than 0.0001 m). Clearly, a full Maxwell model of a realistically long ($\sim$10 m) fiber is beyond the reach of today's simulation capabilities. The need for simplified models is evident. Indeed the state of the art in fiber amplifier simulation consists of beam propagation methods and simplified CMT-based models (see Sect. 2). Yet, even these simplified models are computationally too demanding. This paper contributes to the search for a faster numerical technique by developing a new concept of equivalent short fiber (see Sect. 3) that can speed up these computations a 1000-fold.

The highest power beam combinable amplifiers are large mode area (LMA) circularly symmetric step-index fibers. They have a cylindrical core (usually doped—see Example 2 below) of radius r_{core} and a cladding region enveloping the core extending to radius r_{clad}. We set up our axes so that the longitudinal direction of the fiber is the z-axis. The transverse coordinates will be denoted x, y while using Cartesian coordinates. The refractive index n of the fiber is a piecewise constant function that equals n_{core} in the core and n_{clad} in the cladding. There is also a polymer coating surrounding the inner cladding; however, this will be ignored in our model, which focuses on the guided light in the core region.

At its inlet ($z = 0$ cross section), the fiber core region is seeded by a continuous wave input of highly coherent laser light, which is typically denoted as the "signal". We are interested in how the signal light is amplified by energy transfer from "pump" light while it propagates through the fiber, through the process called "gain". The pump light is also injected at the beginning of the fiber in a "co-pumped" configuration. The signal light is injected into the core, while the pump light goes into both the core and the cladding.

Let $\mathcal{E}_s, \mathcal{H}_s$ and $\mathcal{E}_p, \mathcal{H}_p$ denote the electric and magnetic fields of the signal and pump light, respectively. They are time harmonic of frequencies ω_s and ω_p, respectively, i.e., $\mathcal{E}_\ell(x, y, z, t) = \text{Re}\big[\mathbf{E}_\ell(x, y, z)e^{-\text{i}\omega_\ell t}\big]$, $\mathcal{H}_\ell(x, y, z, t) = \text{Re}\big[\mathbf{H}_\ell(x, y, z)e^{-\text{i}\omega_\ell t}\big]$, for $\ell \in \{s, p\}$, so we may focus on their spatial dependence. We assume that the signal field $\mathbf{E}_s, \mathbf{H}_s$ and the pump field $\mathbf{E}_p, \mathbf{H}_p$ each satisfy the time-harmonic Maxwell system and that they are coupled only through a polarization term $\mathbf{P}_\ell \equiv \mathbf{P}_\ell(\mathbf{E}_s, \mathbf{E}_p)$:

$$\text{curl}\,\mathbf{E}_\ell - \text{i}\omega_\ell\mu_0\mathbf{H}_\ell = 0, \qquad \text{curl}\,\mathbf{H}_\ell + \text{i}\omega_\ell\epsilon_0\mathbf{E}_\ell = -\text{i}\omega_\ell\mathbf{P}_\ell, \qquad \ell \in \{s, p\},$$

where ϵ_0 is the electric permittivity and μ_0 is the magnetic permeability (in vacuum).

Since the fiber is a dielectric medium, the standard linear background polarization term must be taken into account: $\mathbf{P}_\ell^{\text{bg}} = \epsilon_0(n^2 - 1)\mathbf{E}_\ell$. We set the total polarization $\mathbf{P}_\ell$ to $\mathbf{P}_\ell = \mathbf{P}_\ell^{\text{bg}} - \text{i}\epsilon_0\mathbf{E}_\ell n g_\ell c/\omega_\ell$ where the gain term g_ℓ depends

nonlinearly on $\mathbf{E}_s$, $\mathbf{E}_p$ and $c = 1/\sqrt{\epsilon_0\mu_0}$ is the speed of light. Examples of g_ℓ are given below.

Eliminating $\mathbf{H}_\ell$, we obtain the second order equation $\operatorname{curl}\operatorname{curl}\mathbf{E}_\ell - \omega_\ell^2\epsilon_0\mu_0\mathbf{E}_\ell = \omega_\ell^2\mu_0\mathbf{P}_\ell$ for the electric field alone, which by virtue of the expression for $\mathbf{P}_\ell$ simplifies to $\operatorname{curl}\operatorname{curl}\mathbf{E}_\ell - k_\ell^2 n^2\mathbf{E}_\ell + \mathrm{i}k_\ell n g_\ell\mathbf{E}_\ell = 0$ with $k_\ell = \omega_\ell/c$. A further assumption, frequently used in the theory of fiber optics, is that $\mathbf{E}_\ell$ is linearly polarized, i.e., using $\hat{e}_x$ to denote the unit vector in the x-direction, $\mathbf{E}_\ell(x, y, z) = U_\ell(x, y, z)\hat{e}_x$. Its also standard to neglect $\operatorname{grad}\operatorname{div}(U_\ell\hat{e}_x)$ since the dominant variations in $\mathbf{E}_\ell$ are in the z-direction. These assumptions yield the scalar Helmholtz equation for U_ℓ,

$$-\Delta U_\ell - k_\ell^2 n^2 U_\ell + \mathrm{i}k_\ell n g_\ell U_\ell = 0. \tag{1}$$

Examples (below) of g_ℓ we have in mind are expressed in terms of the irradiance $I_\ell = n|U_\ell|^2/\mu_0 c$. Light of high irradiance can perturb the refractive index causing many interesting nonlinear effects in optical fibers, such as in Example 1 below. However, of primary interest to us in the simulation of fiber amplifiers is *active gain*, occurring in fibers whose core is doped with lanthanide rare-earth metallic elements, such as Thulium (Tm) or Ytterbium (Yb)—see Example 2. They result in much larger gain due to the pump light driving dopant ions to excited radiative states followed by stimulated emission into signal photons.

Example 1 (Raman Gain) As described in [7, 10], the nonlinear Raman gain can be modeled using a measurable "bulk Raman gain coefficient" g_R by

$$g_\ell = \Upsilon_\ell g_R I_{\ell^c}, \qquad \ell \in \{s, p\} \tag{2}$$

where $\Upsilon_p = -\omega_p/\omega_s$, $\Upsilon_s = 1$, and $\ell^c \in \{s, p\} \setminus \{\ell\}$, the complementary index of ℓ.

Example 2 (Ytterbium-Doped Fiber) Yb-doped fiber amplifiers are usually pumped at λ_p =976 nm to move ions from a ground state (manifold ${}^2F_{7/2}$) to an excited state (manifold ${}^2F_{5/2}$) [3, 8]. After undergoing a rapid non-radiative transition to a lower energy state, the amplifier can lase around λ_s =1064 nm very efficiently. Denoting the constant, uniformly distributed ion population as $N_{\text{total}} = N_{\text{excited}} + N_{\text{ground}}$, the active gain can be modeled by

$$g_\ell = \sigma_\ell^{\text{ems}} N_{\text{excited}} - \sigma_\ell^{\text{abs}} N_{\text{ground}} = N_{\text{total}}\left[\sigma_\ell^{\text{ems}}\varepsilon - \sigma_\ell^{\text{abs}}(1-\varepsilon)\right] \tag{3}$$

where the excited ion fraction $\varepsilon = N_{\text{excited}}/N_{\text{total}}$ is calculated in terms of a radiative lifetime (τ), and absorption and emission cross sections ($\sigma_\ell^{\text{abs}}, \sigma_\ell^{\text{ems}}$) as $\varepsilon = c^{\text{abs}}/(c^{\text{abs}} + c^{\text{ems}} + \tau^{-1})$, where $c^{\text{e/a}} = \sigma_p^{\text{e/a}} I_p/\hbar\omega_p + \sigma_s^{\text{e/a}} I_s/\hbar\omega_s$, for e/a $\in$ {ems, abs} and $\omega_\ell = 2\pi c/\lambda_\ell$. A commercial Yb-doped fiber, branded Nufern™ (nufern.com), offers realistic parameters for our numerical simulations: $n_{\text{core}} = 1.45097, n_{\text{clad}} = 1.44973, r_{\text{core}} = 12.5$ μm, $r_{\text{clad}} = 16 r_{\text{core}}$. (Other parameters: τ = 8e-4 s; σ_p^{abs}, σ_s^{abs}, σ_p^{ems}, σ_s^{ems} = 1.429e-24, 6e-27, 1.776e-24, 3.58e-25 m^2/ion; N_{total} = 6.25e25 ions/m^3.)

2 CMT Model

Coupled Mode Theory (CMT) uses the *transverse core modes* of the fiber to construct an electric field ansatz. These fiber modes $\varphi_l(x, y)$ are non-trivial functions that, together with their accompanying (positive) *propagation constants* β_l, solve the eigenproblem $(\Delta_{xy} + k_s^2 n^2)\varphi_l = \beta_l^2 \varphi_l$, where $\Delta_{xy} = \partial_{xx} + \partial_{yy}$ denote the transverse Laplacian. Since the modes we expect to see decay exponentially in the cladding region, the eigenproblem may be supplemented with zero Dirichlet boundary conditions. There can only be finitely many such modes, which we index using $l = 1, 2, \ldots, M$. For step-index fibers, these modes are called the linearly polarized (LP) transverse guided core modes [1]. The field ansatz is

$$U_s(x, y, z) = \sum_{m=1}^{M} A_m(z)\varphi_m(x, y)e^{\mathrm{i}\beta_m z}. \tag{4}$$

Furthermore, we assume that each A_m is so slowly varying in z that we may neglect the second derivative $\mathrm{d}^2 A_m/\mathrm{d}z^2$ for all $m = 1, \ldots, M$. Since we may precompute the modes φ_l, the ansatz (4) reduces the field computation to the numerical computation of $A_l(z)$. Substituting (4) into (1) and simplifying using the L^2 orthogonality of the modes, we find that A_l satisfies the system of ordinary differential equations (ODE)

$$\frac{\mathrm{d}A_l}{\mathrm{d}z} = \sum_{m=1}^{M} e^{\mathrm{i}(\beta_m - \beta_l)z}\, K_{lm}(A, I_p)\, A_m, \qquad 0 < z < L, \tag{5}$$

for $l = 1, \ldots, M$, where the mode coupling coefficient K_{lm} is given by

$$K_{lm}(A, I_p) = \frac{k_s}{2\beta_l} \int_{\Omega_z} g_s(I_s(x, y, A), I_p)\, n(x, y)\varphi_m(x, y)\overline{\varphi_l(x, y)}\, dx\, dy. \tag{6}$$

Here Ω_z represents the fiber cross section having the constant longitudinal coordinate value of z. Note that I_s depends on x, y and also on z through $A \equiv \{A_l\}$, i.e., $I_s \equiv I_s(x, y, A) = \frac{n}{\mu_0 c}|\sum_{m=1}^{M} A_m(z)e^{\mathrm{i}\beta_m z}\varphi_m(x, y)|^2$. Note that the "mode beating" term on the right hand side of (5), namely $e^{\mathrm{i}(\beta_m - \beta_l)z}$, oscillates at a wavelength not smaller than the *mode beat length* $2\pi/\max_{l,m}|\beta_m - \beta_l|$. An ODE solver must take enough steps per mode beat length to safeguard accuracy.

As in previous works [6, 9], we use a drastically simplified model of pump light: the effect of pump is modeled only through its irradiance $I_p(z)$ after assuming it to be independent of x and y, leading to the ODE

$$\frac{\mathrm{d}I_p}{\mathrm{d}z} = \langle g_p \rangle I_p \tag{7}$$

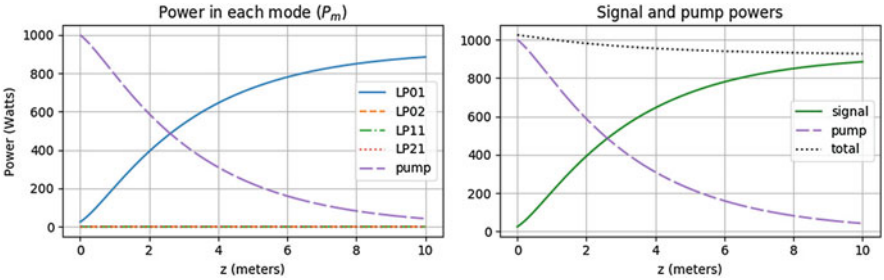

Fig. 1 Results from simulation of the full length ($L = 10$ m) Nufern fiber

where $\langle g_p \rangle(z)$ denotes the mean value of g_p over Ω_z.

Equations (5)–(7) were solved numerically for a 10 m long Nufern fiber of Example 2. This fiber has 4 modes, LP01, LP02, LP11 and LP21, enumerated as $\varphi_1, \ldots, \varphi_4$, respectively. We set initial values $A_m(0)$ such that 25 W of power is injected into the LP01 mode, while the remaining modes receive no power at inlet. Pump light is injected at 1000 W at $z = 0$. Lagrange finite elements of degree 5 were used to approximate φ_l and the mode overlap integral. All our simulations used 50 steps of the 4^{th} order Runge-Kutta scheme per mode beat length. Over 400,000 ODE steps were needed to traverse 10 m. Results are shown in Fig. 1. Clearly, the signal power amplifies as z increases, while the power in pump light depletes.

3 A Scale Model: Equivalent Short Fiber

Physical or numerical scale models of an object preserve some of the important properties of the object while not preserving the original dimensions of the object. In the context of fiber amplifiers, a miniature scale model that reduces fiber length (while preserving the remaining dimensions) would be highly valuable in numerical computations. By reducing the number of steps within the ODE solver, an equivalent shorter fiber can bring about drastic reductions in computational cost.

At the outset, consider a quick dimensional analysis of (5). Its left hand side has dimension V/m (Volts per meter), so K_{lm} must have units of m^{-1}. Therefore, by writing out a non-dimensional formulation, we suspect that a shorter fiber of $\tilde{L} \ll L$ might, in some ways, behave similarly to the original fiber of length L, provided its coupling coefficient is magnified by $L/\tilde{L}$.

We need to understand better in what way the behaviour is similar and what properties need not be preserved. Let $\zeta(\tilde{z}) = \tilde{z}L/\tilde{L}$. A fiber of length L, under the variable change $\tilde{z} = \zeta^{-1}(z) = z\tilde{L}/L$ becomes one of length $\tilde{L}$. The original system (5)–(7) under the variable change, becomes $\mathrm{d}I_p(\tilde{z}L/\tilde{L})/\mathrm{d}\tilde{z} =$

$(L/\tilde{L})\langle g_p\rangle I_p(\tilde{z}L/\tilde{L})$ and

$$\frac{\mathrm{d}}{\mathrm{d}\tilde{z}}A_l(\tilde{z}L/\tilde{L}) = \sum_{m=1}^{M}\frac{L}{\tilde{L}}K_{lm}(A(\tilde{z}L/\tilde{L}),\, I_p(\tilde{z}L/\tilde{L}))\; e^{\mathrm{i}(\beta_m-\beta_l)(L/\tilde{L})\tilde{z}}\, A_m(\tilde{z}L/\tilde{L}), \tag{8}$$

for all $0 < \tilde{z} < \tilde{L}$. Letting $\hat{A}_l = A_l \circ \zeta$ and $\hat{I}_p = I_p \circ \zeta$, we may rewrite these as

$$\frac{\mathrm{d}\hat{A}_l}{\mathrm{d}\tilde{z}} = \sum_{m=1}^{M} e^{\mathrm{i}(\beta_m-\beta_l)L\tilde{z}/\tilde{L}}\,\frac{L}{\tilde{L}}\,K_{lm}(\hat{A},\hat{I}_p)\;\hat{A}_m, \quad \frac{\mathrm{d}\hat{I}_p}{\mathrm{d}\tilde{z}} = \frac{L}{\tilde{L}}\langle g_p\rangle\hat{I}_p, \quad 0 < \tilde{z} < \tilde{L}. \tag{9}$$

Thus, (9) on the shorter domain $0 < \tilde{z} < \tilde{L}$ is completely equivalent to (5)–(7). (Same initial data at $z = \tilde{z} = 0$ is assumed throughout.) Indeed, its solution $\hat{A}_l$, after changing variables is the same as the original solution A_l of (5). Unfortunately, (9) is not an improvement over (5) for numerical simulation. This is because the mode beat length is now reduced by $\tilde{L}/L$ in (9). Therefore an ODE solver, keeping the same number of steps per mode beat length, must now perform $L/\tilde{L}$ times the number of original steps, thus destroying the advantage of shortening the fiber to length $\tilde{L}$.

Hence we formulate another mode coupling system on the shorter fiber, with the same mode beat length as the original system (5)

$$\frac{\mathrm{d}\tilde{A}_l}{\mathrm{d}\tilde{z}} = \sum_{m=1}^{M} e^{\mathrm{i}(\beta_m-\beta_l)\tilde{z}}\frac{L}{\tilde{L}}K_{lm}(\tilde{A},\tilde{I}_p)\tilde{A}_m, \quad \frac{\mathrm{d}\tilde{I}_p}{\mathrm{d}\tilde{z}} = \frac{L}{\tilde{L}}\langle g_p\rangle\tilde{I}_p, \quad 0 < \tilde{z} < \tilde{L}. \tag{10}$$

Since the phase factors in (9) and (10) are different, we cannot expect $\tilde{A}_l(\tilde{z})$ to be the same as the pullback $A_l \circ \zeta$ of the original solution A_l. Thus (10) is not completely equivalent to the original system (5): it does not preserve the solution. Yet the phase information lost in this new formulation is not of significant importance experimentally. Hence, we proceed to argue that (10) is a practically useful scale model of (5) by showing that it preserves some features of the solution under certain conditions.

Let $a_l(z) = A_l(z)e^{\mathrm{i}\beta_l z}$. Elementary calculations show that (5) implies

$$\frac{\mathrm{d}|a_l|^2}{\mathrm{d}z} = 2\sum_{m=1}^{M}\mathrm{Re}\big[K_{lm}(A,I_p)\,\overline{a}_l a_m\big]. \tag{11}$$

Let P be the vector function whose l^{th} component, $P_l(z)$, is the power contained in the l^{th} mode, namely $P_l(z) = \int_{\Omega_z}\frac{n}{\mu_0 c}|A_l(z)\varphi_l(x,y)|^2\,dx\,dy = |a_l|^2\Phi_l$, where

$\Phi_l = \int_{\Omega_z} \frac{n}{\mu_0 c} |\varphi_l|^2 \, dx \, dy$. Equation (11) can be expressed using P_l as

$$\frac{1}{2}\frac{\mathrm{d}P_l}{\mathrm{d}z} = K_{ll}(A, I_p)P_l + \Phi_l \sum_{m \neq l} \mathrm{Re}\big[K_{lm}(A, I_p)\,\overline{a}_l a_m\big]. \tag{12}$$

Recall that $K_{lm}(A, I_p)$ is defined using $g_s(I_s(x, y, A), I_p)$—see (6). In some circumstances (see below), $I_s(x, y, A) = \frac{n}{\mu_0 c} |\sum_{m=1}^{M} a_m \varphi_m|^2$ can be approximated by

$$\mathcal{I}_s(P) = \sum_{m=1}^{M} \frac{n}{\mu_0 c} |a_m \varphi_m|^2 = \sum_{m=1}^{M} \frac{n}{\mu_0 c \Phi_m} P_m \, |\varphi_m|^2 .$$

Let $\gamma_\ell(P, I_p) = g_\ell(\mathcal{I}_s(P), I_p)$ for $\ell \in \{s, p\}$ and let κ_{lm} be defined exactly as K_{lm} but with g_s replaced by γ_s. Then (12) may be rewritten as

$$\frac{1}{2}\frac{\mathrm{d}P_l}{\mathrm{d}z} = \kappa_{ll}(P)P_l + \eta_l, \qquad l = 0, 1, \ldots, M, \qquad \text{where} \tag{13}$$

$$\eta_l = \Big[K_{ll}(A, I_p) - \kappa_{ll}(P)\Big]P_l + \Phi_l \sum_{m \neq l} \mathrm{Re}\Big[K_{lm}(A, I_p)\,\overline{a}_l a_m\Big] \tag{14}$$

for $l = 1, \ldots, M$. For the index $l = 0$, we set $P_0(z) = \int_{\Omega_z} I_p(z) \, dxdy$, the pump power, thereby absorbing (7) into (13) after setting $\eta_0 = \frac{1}{2}\big[\langle g_p \rangle - \langle \gamma_p \rangle\big]P_0$. We are interested in the case of small η_l. Then (13) is a perturbation of an autonomous system.

Repeating the same procedure starting from (10) using $\tilde{a}_l(z) = \tilde{A}_l(z)e^{\mathrm{i}\beta_l z}$, we find that the corresponding powers $\tilde{P}_l = |\tilde{a}_l|^2 \Phi_l$ and $\tilde{P}_0 = \int_{\Omega_z} \tilde{I}_p \, dx \, dy$ satisfy

$$\frac{1}{2}\frac{\mathrm{d}\tilde{P}_l}{\mathrm{d}\tilde{z}} = \frac{L}{\tilde{L}}\kappa_{ll}(\tilde{P})\tilde{P}_l + \tilde{\eta}_l, \qquad l = 0, 1, \ldots, M, \qquad \text{where} \tag{15}$$

$$\tilde{\eta}_l = \left[\frac{L}{\tilde{L}}K_{ll}(\tilde{A}, \tilde{I}_p) - \frac{L}{\tilde{L}}\kappa_{ll}(\tilde{P})\right]\tilde{P}_l + \Phi_l \sum_{m \neq l} \mathrm{Re}\left[\frac{L}{\tilde{L}}K_{lm}(\tilde{A}, \tilde{I}_p)\,\overline{\tilde{a}}_l \tilde{a}_m\right].$$

To compare (15) with (13), we apply the change of variable ζ to (13) to find that $\frac{1}{2}\mathrm{d}(P_l \circ \zeta)/\mathrm{d}\tilde{z} = (L/\tilde{L})\kappa_{ll}(P_l \circ \zeta)P_l \circ \zeta + (L/\tilde{L})\eta_l \circ \zeta$. This means that when η and $\tilde{\eta}$ are small, $P_l \circ \zeta$ and $\tilde{P}_l$ solve approximately the same equation, so $P_l \circ \zeta \approx \tilde{P}_l$.

For this reason we shall call (10) an *equivalent short fiber model,* even if the electric fields generated are generally not the same. Note that, when considering real fiber amplifiers, power is the quantity of interest (measurable experimentally), not the electric field amplitude and phase. To summarize, *in the equivalent short fiber, the power P_l contained in the l^{th} mode is preserved from the original fiber model* (5) through a change of variable, under the above assumptions. Moreover, by

estimating $\tilde{\eta}$ in equivalent fiber computations, we can gauge the reliability of the equivalent short fiber model a posteriori.

To simulate the equivalent short fiber model (10), we only need to multiply K_{lm} and $\langle g_p \rangle$ by $L/\tilde{L}$. In Example 1, this is accomplished by scaling the bulk Raman gain coefficient, i.e., replace the physical g_R by $\tilde{g}_R = g_R L/\tilde{L}$ in (2). Whereas for an active gain amplifier (like that of Example 2) this may be accomplished by scaling the total number of dopant ions, i.e., by replacing the physical N_{total} by $\tilde{N}_{\text{total}} = N_{\text{total}} L/\tilde{L}$.

One scenario where the assumption that η is small is justified is when most of the power is carried in one mode. Indeed, typical experimental setups of LMA fiber amplifiers do operate them as near-single mode fibers by filtering out the higher-order modes through differential bend losses induced by fiber coiling. When all except one a_i is small, cross terms involving $\bar{a}_l a_m$ are small for all $l \neq m$, so the last term in (14) is small. Moreover, the approximation of I_s by $\mathcal{I}_s$ where similar cross terms are neglected, is also accurate, so all terms defining (14) are small.

Figure 2 shows simulation results from the equivalent short fiber model of length $\tilde{L} = 0.01$ m mimicking the physical Nufern fiber of length $L = 10$ m we simulated at the end of Sect. 2. We see that the power distribution plots (bottom row) are identical to that of the physical fiber in Fig. 1. The cost of computation has however been reduced by a factor of $\tilde{L}/L = 1/1000$ (keeping the same number of ODE steps per mode beat length, see Sect. 2). When $\tilde{L}$ is changed to 0.005—see Fig. 3—we obtain similar power distribution plots again, although the solution components (A_m) have notably changed, in agreement with our analysis above. In further experiments (unreported here for brevity), we observed good performance

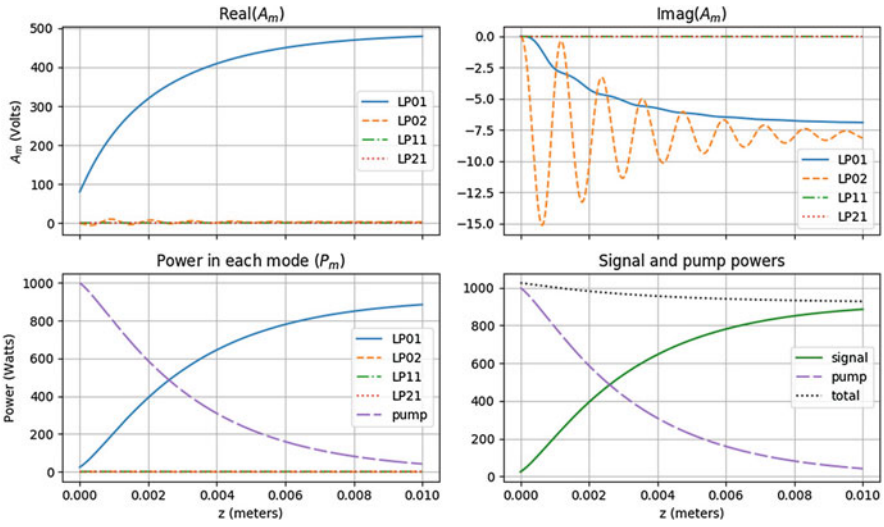

Fig. 2 Results from a short fiber of length $\tilde{L} = 0.01$ equivalent to an $L = 10$ m Nufern fiber

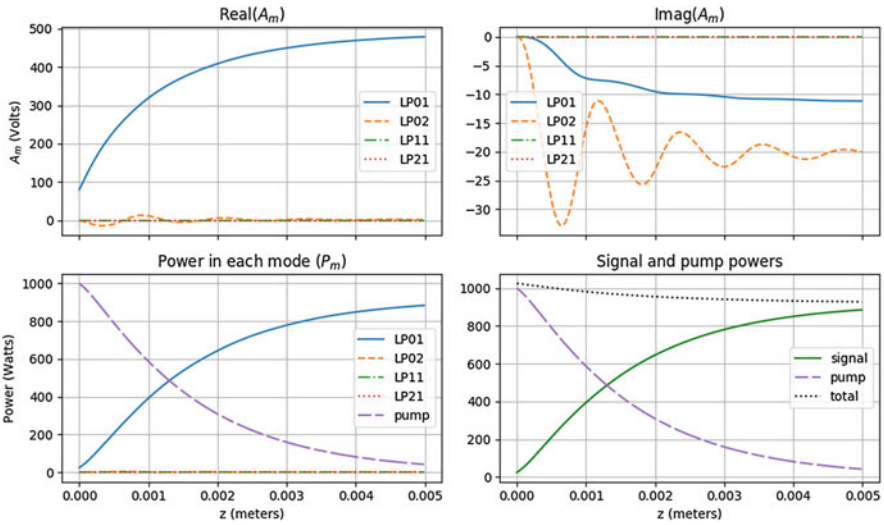

Fig. 3 Results from a short fiber of length $\tilde{L} = 0.005$ equivalent to an $L = 10$ m Nufern fiber

of equivalent fiber of length 0.1 m even when power was distributed equally among the modes. Note that all our simulations considered the worst-case scenario of no differential mode bend loss, i.e., any tendency of a bent fiber toward single-mode operation is left unmodeled.

Acknowledgments This work was supported in part by AFOSR grant FA9550-17-1-0090.

References

1. Agrawal, G.P.: Nonlinear Fiber Optics, 5th edn. Elsevier, New York (2013)
2. Eidam, T., Wirth, C., Jauregui, C., Stutzki, F., Jansen, F., Otto, H., Schmidt, O., Schreiber, T., Limpert, J., Tünnermann, A.: Experimental observations of the threshold-like onset of mode instabilities in high power fiber amplifiers. Opt. Express **19**(14), 13218–13224 (2011)
3. Grosek, J., Naderi, S., Oliker, B., Lane, R., Dajani, I., Madden, T.: Laser simulation at the Air Force Research Laboratory. In: Proc. SPIE, vol. 10254, p. 102540N-1 (2017)
4. Jauregui, C., Limpert, J., Tünnermann, A.: High-power fibre lasers. Nat. Photonics **7**(11), 861–867 (2013)
5. Jauregui, C., Otto, H.-J., Stutzki, F., Limpert, J., Tünnermann, A.: Simplified modelling the mode instability threshold of high power fiber amplifiers in the presence of photodarkening. Opt. Express **23**(16), 20203–20218 (2015)
6. Naderi, S., Dajani, I., Madden, T., Robin, C.: Investigations of modal instabilities in fiber amplifiers through detailed numerical simulations. Opt. Express **21**(13), 16111–16129 (2013)
7. Nagaraj, S., Grosek, J., Petrides, S., Demkowicz, L., Mora, J.: A 3D DPG Maxwell approach to nonlinear Raman gain in fiber laser amplifiers. Preprint, arXiv:1805.12240 (2018)

8. Pask, H., Carman, R., Hanna, D., Tropper, A., Mackechnie, C., Barber, P., Dawes, J.: Ytterbium-doped silica fiber lasers: versatile sources for the 1-1.2 μm region. IEEE J. Sel. Top. Quantum Electron. **1**(1), 2–13 (1995)
9. Smith, A.V., Smith, J.J.: Mode instability in high power fiber amplifiers. Opt. Express **19**(11), 10180–10192 (2011)
10. Verdeyen, J.T.: Laser Electronics, 3rd edn. Prentice Hall, Englewood Cliffs (1995)